J. Space Weather Space Clim. 2022, **12**, 6

https://doi.org/10.1051/swsc/2022005

JSWSC

Available online at:
www.swsc-journal.org

RESEARCH ARTICLE OPEN ACCESS

Responding trends of ionospheric F_2-layer to weaker geomagnetic activities

Yiding Chen[1,2,3,4,*], Libo Liu[1,2,4,5], Huijun Le[1,2,4,5], Hui Zhang[1,2,4,5], and Ruilong Zhang[1,2,4,5]

[1] Key Laboratory of Earth and Planetary Physics, Institute of Geology and Geophysics, Chinese Academy of Sciences, Beijing 100029, PR China
[2] Innovation Academy for Earth Science, CAS, Beijing 100029, PR China
[3] Beijing National Observatory of Space Environment, Institute of Geology and Geophysics, Chinese Academy of Sciences, Beijing 100029, PR China
[4] College of Earth and Planetary Sciences, University of Chinese Academy of Sciences, Beijing 100049, PR China
[5] Heilongjiang Mohe Observatory of Geophysics, Institute of Geology and Geophysics, Chinese Academy of Sciences, Beijing 100029, PR China

Received 18 September 2021 / Accepted 22 February 2022

Abstract – Geomagnetic activities frequently occur in varying degrees. Strong geomagnetic activities, which have been widely investigated, occur occasionally; they can cause distinguishable and significant disturbances in the ionosphere. Weaker geomagnetic activities frequently appear, whereas their effects are generally difficult to be distinguished from complex ionospheric variations. Weaker geomagnetic activities play important roles in ionospheric day-to-day variability thus should deserve further attention. In this study, long-term (longer than one solar cycle) measurements of the F_2-layer critical frequency (f_oF_2) were collected to statistically investigate ionospheric responses to weaker geomagnetic activities ($Ap < 60$). The responding trends of low- to high-latitude f_oF_2 to increasing geomagnetic activity are presented for the first time; they are statistically evident. Both increasing and decreasing trends can occur, depending on latitudes and seasons. The trend gradually transits from high-latitude decreasing trends to equatorial increasing trends with decreasing latitude, and this transition is seasonally dependent. As a result, the trend has a seasonal difference at mid-latitudes. The responding trend is generally more distinct at higher latitudes and in the equatorial region than at mid-latitudes, and the responding intensity is largest at higher latitudes. Although theoretically, geomagnetic activities can disturb the ionosphere through multiple mechanisms, the morphology of the trend suggests that the frequent weaker geomagnetic activities modulate the high- to low-latitude ionosphere mainly through disturbing high-latitude thermospheric composition and further altering the thermospheric background circulation.

Keywords: ionospheric disturbance / weaker geomagnetic activity / responding trend / thermospheric composition

1 Introduction

The ionosphere closely couples with the magnetosphere and solar wind, it can be significantly disturbed when the energy from the magnetosphere and solar wind deposits into the high-latitude ionosphere and upper atmosphere. In general, this energy deposition is very frequent, usually weaker while occasionally strong. Accompanying this energy deposition, the space current system, including ionospheric current, is disturbed. As a result, the magnetic field measured on the ground is disturbed, and the disturbance degree is positively related to the energy deposition. Thus, various geomagnetic activity indices (e.g., Mayaud, 1980) were developed from ground-based magnetic field measurements to estimate the strength of the energy deposition. Geomagnetic activity indices have been widely used for space physics studies and space weather applications.

Strong geomagnetic activities, which manifest as intense variations of geomagnetic activity indices, usually result in considerable disturbances in the global ionosphere, i.e., ionospheric storms. Ionospheric storms have become a very active topic and have been widely investigated since they were discovered (Anderson, 1928; Hafstad & Tuve, 1929), owing to their remarkable influences on the space environment. Many disturbance processes were suggested to be responsible for ionospheric storms, such as storm-time changes in high-latitude particle precipitation and plasma convection, thermospheric composition, neutral winds, and ionospheric electric fields. The combined effects of these disturbance processes make

*Corresponding author: chenyd@mail.iggcas.ac.cn

ionospheric storm changes very complicated. Ionospheric disturbance morphologies during different storm events may be very discrepant, while statistically, there were some regular features. These have been well summarized in some review papers (e.g., Prölss, 1995; Buonsanto, 1999; Mendillo, 2006; Danilov, 2013).

Compared with the ionospheric storms, weaker geomagnetic activities occur very frequently, while ionospheric responses to weaker geomagnetic activities were much less investigated. One reason is that it is usually difficult to distinguish the effects of weaker geomagnetic activities from the complex ionospheric day-to-day variability caused simultaneously by solar irradiance, geomagnetic activities, and waves from the lower atmosphere (e.g., Forbes et al., 2000; Rishbeth & Mendillo, 2001; Mendillo et al., 2002). Moreover, unlike ionospheric storms dominated by separated major geomagnetic disturbances, the frequent occurrence of weaker geomagnetic activities (as shown in Fig. 1a for an example) makes it very difficult to distinguish the effects of different disturbances. Even so, the effects of weaker geomagnetic activities can be identified under some particular conditions. The corotating interaction regions associated with solar wind high-speed streams can cause recurrent geomagnetic activities with weak-to-moderate strength (e.g., Gonzalez et al., 1999; Tsurutani et al., 2006a, 2006c). Geomagnetic activity can enhance and then decline for days repeatedly during recurrent geomagnetic activity periods, which may result in the quasi-periodic ionospheric disturbance. This periodic disturbance can be identified from the complex ionospheric day-to-day variability (e.g., Lei et al., 2008; Pedatella et al., 2010; Tulasi Ram et al., 2010; Wang et al., 2011) if it is not synchronous with other ionospheric disturbances induced by other factors. Solar activity was very low, so solar irradiance was relatively steady during the 2007–2009 deep solar minimum, which increases the importance of geomagnetic activities to ionospheric day-to-day variability thus is propitious for detecting the effects of weaker geomagnetic activities. Buresova et al. (2014) analyzed the effects of a set of weaker geomagnetic disturbances on the mid-latitude ionosphere during the 2007–2009 deep solar minimum. They found that the effects of weaker geomagnetic disturbances during that period were compared with those of stronger storms under higher solar activity conditions, with the prevalence of positive ionospheric disturbances. Chen et al. (2014a) reported that day-to-day variations of the global electron content were well positively correlated with the *Ap* index during 2007–2009. This positive correlation implies that as far as long-term ionospheric variation is concerned, the more declining geomagnetic activity in 2007–2009 than during previous solar minima (e.g., Chen et al., 2011) may contribute to the decreasing electron density in that period to some extent. Solomon et al. (2013, 2018) and Emmert et al. (2017) investigated the contribution of the declining geomagnetic activity during 2007–2009 to the decrement of globally averaged electron density.

Although ionospheric responses to weaker geomagnetic activities under those particular conditions, such as recurrent geomagnetic activities and the deep solar minimum, have been analyzed, it is still a challenge to directly identify the effect of ordinary weaker geomagnetic disturbances on the ionosphere from observations. That effect frequently acts on the ionosphere and is an important contributor to ionospheric complex variability; it should deserve further investigation. In this study,

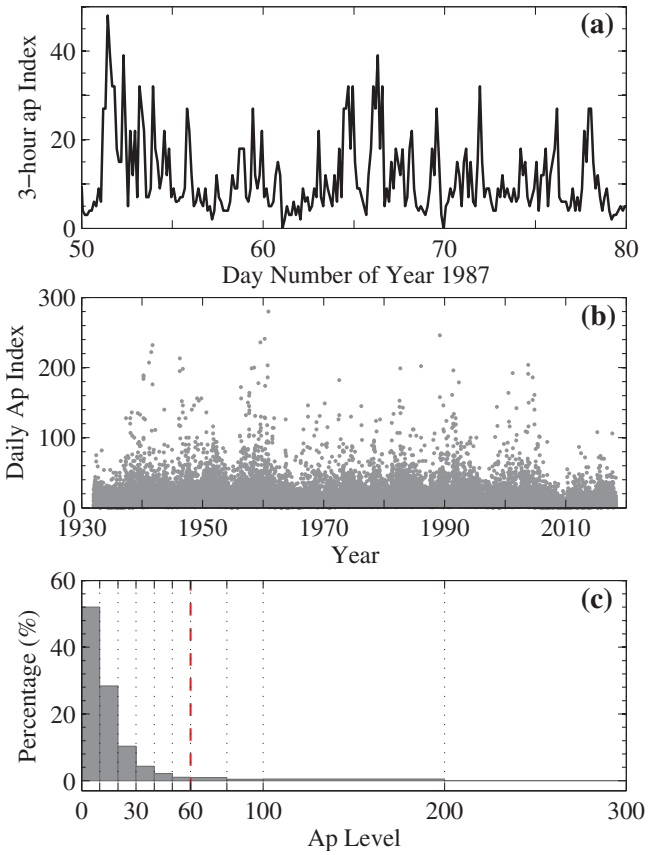

Fig. 1. (a) A segment of the 3-h *ap* index showing frequent occurrence of weaker geomagnetic activities; (b) time series of the daily *Ap* index; (c) percentages of different geomagnetic activity levels indicated by *Ap* ranges.

long-term ionosonde measurements covering geomagnetic low- to high-latitudes were collected to statistically analyze the responses of the F_2-layer critical frequency (f_oF_2) to weaker geomagnetic activities, instead of case analyses. The responding trends of low- to high-latitude f_oF_2 to increasing geomagnetic activity were obtained for the first time after carefully removing the contributions of the factors such as varying solar irradiance and background seasonal variations. Figure 1b shows the time series of the *Ap* index, and Figure 1c presents the percentages of different *Ap* ranges to examine the distribution of geomagnetic activity. It can be seen that *Ap* changes very frequently and is mainly at the level of tens. In this paper, the weaker geomagnetic activity refers to the level of $Ap < 60$. It should be noted that the used data are mainly at the geomagnetic activity level of $Ap < 30$ (as shown in Fig. 1c).

2 Data analysis method and results

In view of the difficulty of distinguishing the effects of separated weaker geomagnetic disturbances from ionospheric day-to-day variability, we statistically analyzed ionospheric responding trends to weaker geomagnetic activities using long-term f_oF_2 data measured by ionosondes. These ionosondes are mainly in the East Asia–Australia longitude sector and

Table 1. Information of the ionosonde stations and data.

Station name	Geographic location	Magnetic latitude	Year coverage of data
Dikson	80.4° E, 73.5° N	63.2° N	1957–1959, 1982–1986, 1988–2001
Norilsk	88.1° E, 69.4° N	58.7° N	1968–1988
Yakutsk	129.6° E, 62.0° N	51.3° N	1957–1989, 1991
Petropavlovsk	158.7° E, 53.0° N	45.0° N	1968–1974, 1989–2006
Irkutsk	104.0° E, 52.5° N	41.3° N	1957–1992, 1996–1997
Wakkanai	141.7° E, 45.4° N	35.7° N	1948–1988, 1992–1993, 1996–2018
Kokubunji	139.5° E, 35.7° N	25.9° N	1957–2018
Yamagawa	130.6° E, 31.2° N	20.7° N	1957–1988, 1996–1999, 2001–2018
Okinawa	127.8° E, 26.3° N	15.6° N	1957–1989, 1992–1993, 1996–2018
Manila	121.1° E, 14.7° N	3.7° N	1964–1994, 1999
Kodaikanal	77.5° E, 10.2° N	0.6° N	1957–1987
Singapore	103.8° E, 1.3° N	9.8° S	1957–1971
Darwin	131.0° E, 12.5° S	22.9° S	1982–2009
Townsville	146.9° E, 19.7° S	28.4° S	1951–1994, 1997, 2003–2009
Brisbane	152.9° E, 27.5° S	35.3° S	1950–1986, 2002–2009
Canberra	149.1° E, 35.3° S	43.5° S	1950–1994, 2003–2009
Hobart	147.3° E, 42.9° S	51.2° S	1950–1959, 1962–1994, 1999, 2003–2009
Macquarie Is	159.0° E, 54.5° S	60.6° S	1950–1958, 1983–1992, 2003–2009
Terre Adelie	140.0° E, 66.7° S	75.2° S	1959, 1964–1986
Casey	110.6° E, 66.3° S	77.5° S	1957–1975, 1990–1992, 2004–2009
Scott Base	166.8° E, 77.9° S	78.8° S	1958–1959, 1970–1983, 2003–2006

distribute over high northern latitudes to high southern latitudes (see Table 1 for details; 9 stations in the northern hemisphere, 9 stations in the southern hemisphere, and 3 stations in the geomagnetic equatorial region) so that latitudinal features of the responding trend can be investigated in detail. These ionosondes continuously or piecewise continuously measured f_oF_2 variations.

The recorded f_oF_2 variations include both the longer-term variations, such as the solar cycle and seasonal variations and the short-term variations, such as the day-to-day and diurnal variations. The longer-term variations are dominant; they should be removed in order to investigate geomagnetic activity effects. The solar forcing contributes to the solar cycle variation and the short-term day-to-day variation of the ionosphere. The short-term solar forcing effects also should be removed to identify geomagnetic activity effects. Although solar extremely ultraviolet (EUV) irradiance ionizes the upper atmosphere to form the ionosphere, it was not continuously measured. Thus, for historical ionospheric measurements, various solar proxies such as the widely used $F_{10.7}$ (the solar 10.7 cm radio flux) index were usually used to estimate the solar forcing to the ionosphere. The solar cycle effects of EUV can be well captured in terms of nonlinear fittings of ionospheric electron density versus solar proxies (e.g., Chen et al., 2008, 2014b; Sethi et al., 2002; Elias, 2014). However, for short-term EUV variation, solar proxies do not work as well as they do for the solar cycle variation. Vaishnav et al. (2019) found that the He II is the best solar proxy for total electron content variations on the time scales of weeks. Whereas the He II data set, do not cover the whole time interval of the ionospheric measurements used in this study. Chen et al. (2012) found that the short-term EUV versus $F_{10.7}$ slope is variable and significantly lower than the solar cycle EUV versus $F_{10.7}$ slope. They accordingly improved the $F_{10.7}$ index by weighting short-term and solar cycle $F_{10.7}$ variations to eliminate the EUV versus $F_{10.7}$ slope difference between short-term and solar cycle timescales. The ability of the improved index for estimating EUV was promoted as compared with daily $F_{10.7}$. A similar improved index was used in other studies (e.g., Richards et al., 1994; Liu et al., 2006). Furthermore, short-term EUV and $F_{10.7}$ variations were found to be nonsynchronous (e.g., Woods et al., 2005; Chen et al., 2018); $F_{10.7}$ variation leads EUV variation with a typical time shift of 1 day for daily EUV and $F_{10.7}$. This should be taken into account when estimating solar EUV using the $F_{10.7}$ index. Thus, we used the following weighted index of $F_{10.7}$ (the S index) to more accurately estimate solar EUV according to Chen et al. (2012), with a 1-day lag of EUV to $F_{10.7}$ (Chen et al., 2018) being taken into account:

$$S = (0.4F_{10.7} + 0.6F_{10.7A})_p, \quad (1)$$

where $F_{10.7A}$ is the 81-day running average of $F_{10.7}$, the subscript 'p' means the value of the preceding day. Figures 2a and 2b present the effectiveness of the weighted index S for improving solar EUV estimation. The EUV flux was measured by the Solar EUV Monitor aboard the Solar Heliospheric Observatory satellite (SOHO/SEM) (Judge et al., 1998).

Daytime f_oF_2 responses to weaker geomagnetic activities were investigated as the representative. Five hourly f_oF_2 values around local noon in each day were averaged to obtain a mean midday f_oF_2 value (see Table 1 for the year coverage of the data). By doing this, some transitory ionospheric fluctuations such as those associated with atmospheric waves may be suppressed to some extent to highlight geomagnetic activity effects. A cubic function of S was used to remove the solar forcing from the mean midday f_oF_2. Some studies indicated there are time lags in the F_2-layer responses to solar EUV variations (e.g., Rich et al., 2003; Min et al., 2009; Coley & Heelis, 2012; Chen et al., 2015; Vaishnav et al., 2019). Accordingly, a 1-day lag of f_oF_2 to the S index was included in the function. In general, ionospheric seasonal variations are dominated by the annual

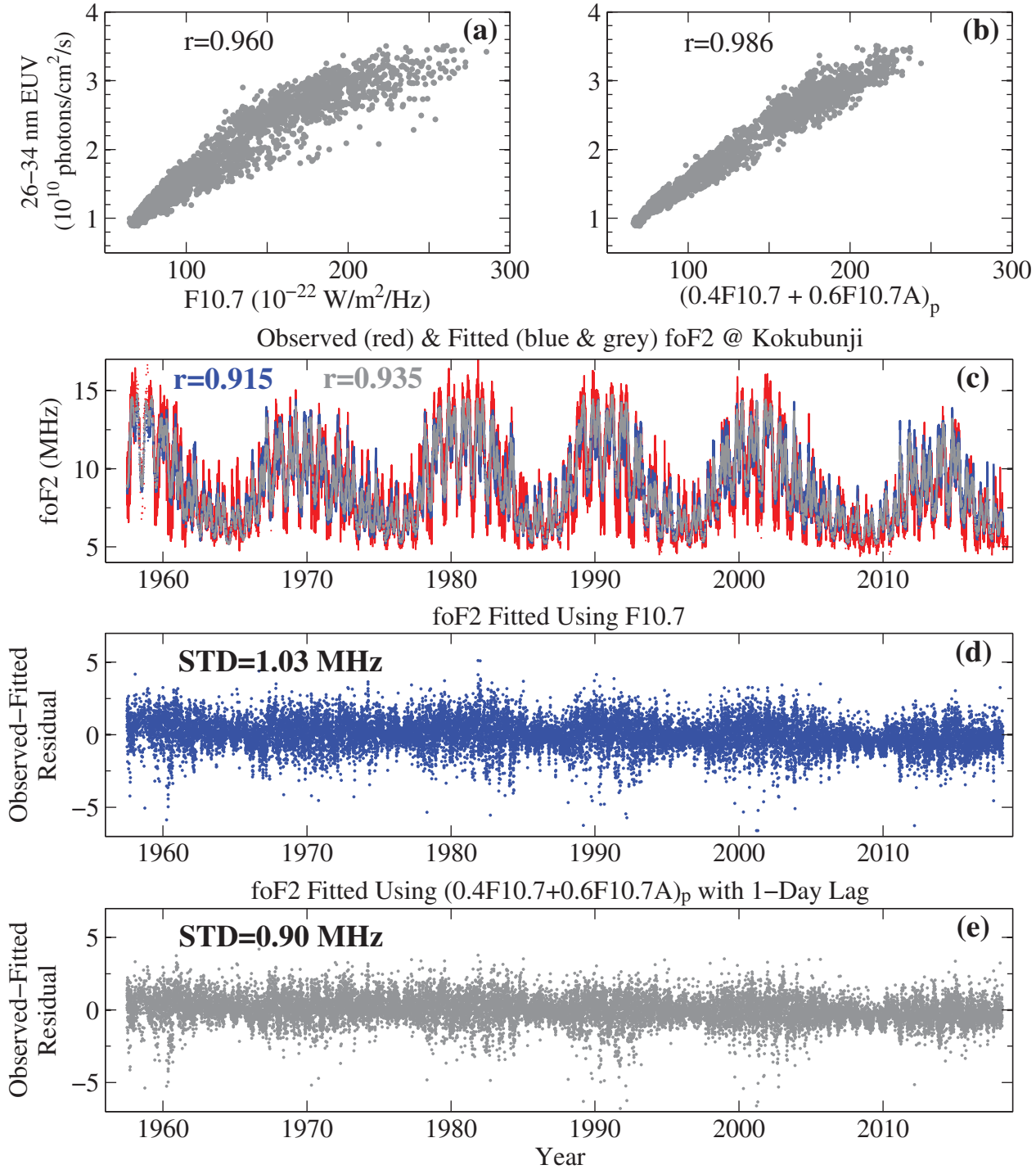

Fig. 2. Scatter plots of daily SOHO/SEM 26-34 nm EUV flux versus (a) the $F_{10.7}$ index and versus (b) the *S* index during the solar cycle 23; the parameter *r* is the correlation coefficient between the EUV flux and the indices. (c) Variations of mean midday f_oF_2 at Kokubunji; the red line for observed values, the blue line for $F_{10.7}$ fitted values, and the grey line for the *S* index fitted values with 1–day lag of f_oF_2 to *S* being included; *r* is the correlation coefficient between observed and fitted f_oF_2. (d) Difference between observed and $F_{10.7}$ fitted f_oF_2; the parameter *STD* is the standard deviation of the difference. (e) Same as Figure 2d but for the *S* index fitted f_oF_2.

and semiannual components (e.g., Liu et al., 2009); some researchers also noted the terannual component (e.g., Xu et al., 2012). A third-order Fourier decomposition was applied to the data series of f_oF_2 to capture the seasonal variations. Thus, the mean midday f_oF_2 was fitted according to equation (2) to remove the solar forcing and seasonal variations:

$$f_oF_2 = \sum_{n=0}^{3} \left[\begin{array}{l} \left(a_n {S_p}^3 + b_n {S_p}^2 + c_n S_p + d_n\right) \cdot \cos\left(\frac{2\pi n \cdot \mathrm{DoY}}{365}\right) + \\ \left(e_n {S_p}^3 + f_n {S_p}^2 + g_n S_p + h_n\right) \cdot \sin\left(\frac{2\pi n \cdot \mathrm{DoY}}{365}\right) \end{array} \right], \quad (2)$$

Where S_p is the S value of the preceding day; DoY means day number of year. The solar forcing is included in the Fourier coefficients. Figure 2c shows the observed and fitted mean midday f_oF_2 at Kokubunji as an example; f_oF_2 was fitted using the $F_{10.7}$ index and the S index (with 1-day lag of f_oF_2 to S) respectively for comparison. Both fittings can well capture the observed solar cycle and seasonal variations of f_oF_2, while they differ obviously on short-term timescales owing to their discrepant abilities for estimating the short-term solar forcing. The S index fitting is more correlated with the observed f_oF_2 than the $F_{10.7}$ fitting. Geomagnetic activity effects are included in the residual of the observed minus fitted f_oF_2, as shown in Figures 2d and 2e. Consistent with Figure 2c, the standard deviation of the S index fitting residual is smaller than the $F_{10.7}$ fitting residual, indicating the S index can remove the solar forcing more adequately than $F_{10.7}$. Thus, the S index fitting residual, Δf_oF_2, was used to analyze the effects of weaker geomagnetic activities.

There are various geomagnetic activity indices serving different purposes (e.g., Mayaud, 1980), while they are statistically correlated. The *Dst* index can be used as a good indicator for different stages of magnetic storms, especially for stronger storms. The *AE* index mainly serves as an indicator of the substorm process occurring at high latitudes. The *ap* index has a long record; it has been made available since 1932. Both magnetic storms and substorms can result in corresponding changes of *ap* and potentially cause global ionospheric disturbances. Studies have revealed that statistically *ap* variation is a synthesis of *AE* and *Dst* to some extent (e.g., Gonzalez et al., 1994; Fares Saba et al., 1997), although it is not an ideal indicator for the energy deposition process of storms or substorms. In this study, the *ap* index and its daily mean *Ap* were used since some ionosonde measurements started as early as 1948 when *Dst* and *AE* were unavailable.

The ionosphere can be disturbed for a period of time after each geomagnetic disturbance process. Strong geomagnetic activities are usually separated; thus, ionospheric response to each disturbance process can be investigated. As shown in Figure 1a, weaker geomagnetic activities sometimes occur very frequently, so the effects of different disturbances on the ionosphere interwork. Thus, averages of geomagnetic activity indices, for example, the daily *Ap* index, are usually used to evaluate mean disturbance levels to investigate ionospheric variations. We used the average of the eight 3-h *ap* values preceding the local noon of f_oF_2 measurement day, $\langle ap \rangle_{24\ \mathrm{h}}$, to estimate the mean geomagnetic activity level responsible for f_oF_2 disturbances. Since the objective of this study is ionospheric responses to weaker geomagnetic activities, the data were excluded if *Ap* was larger than 60 on the f_oF_2 measurement day or on the preceding day. The data were further divided into four groups to investigate the seasonal dependence of the ionospheric response. Each group includes the measurements of ±30 days centered on the equinox or solstice day to represent different seasonal conditions.

Figure 3 shows the scatter plots of Δf_oF_2 versus $\langle ap \rangle_{24\ \mathrm{h}}$ at Petropavlovsk as an example. Δf_oF_2 shows decreasing trends with increasing geomagnetic activity in two equinoxes and June solstice, while it trends to increase first and then decrease with increasing $\langle ap \rangle_{24\ \mathrm{h}}$ in December solstice. The data points are scattered around the trends and distribute unevenly over different $\langle ap \rangle_{24\ \mathrm{h}}$ levels. Δf_oF_2 data were further normalized to regular $\langle ap \rangle_{24\ \mathrm{h}}$ grids using a moving window of 10 with a steplength of 5 in order to more directly present the trends. The red dots in Figure 3 are mean values of the gridded data, and the error bars are corresponding lower and upper quartiles. The gridded Δf_oF_2 somewhat increases first and then declines with increasing $\langle ap \rangle_{24\ \mathrm{h}}$ in December solstice. The decreasing trends of the gridded Δf_oF_2 are evident in other seasons. The correlation coefficients between Δf_oF_2 and $\langle ap \rangle_{24\ \mathrm{h}}$ were calculated. Higher correlation coefficients mean more regular responses of f_oF_2 to weaker geomagnetic disturbances. Consistent with the trends, the correlation coefficient is negative except for that in the December solstice, it can reach −0.53 in September equinox. The correlation is insignificant in December solstice since the increasing trend gradually changes into the decreasing trend with increasing geomagnetic activity.

We analyzed all of the measurements at 21 stations and found that the responding trend of Δf_oF_2 to increasing geomagnetic activity significantly depends on latitudes and has obvious seasonal differences at mid-latitudes. Figure 4 presents the trends of the gridded Δf_oF_2 with increasing $\langle ap \rangle_{24\ \mathrm{h}}$ at the northern hemisphere stations. Δf_oF_2 decreases with increasing $\langle ap \rangle_{24\ \mathrm{h}}$ at higher latitudes (Dikson, Norilsk, and Yakutsk). The responding trend changes gradually with decreasing latitude. It turns to increase trends first in local winter (see Petropavlovsk, the increasing trend begins to appear at the low disturbance level of $\langle ap \rangle_{24\ \mathrm{h}}$<20) and then in equinoxes (see Kokubunji and Yamagawa), while it maintains the decreasing trend in local summer. The increasing trends in winter become evident at lower latitudes. This latitudinal transition of the responding trend also takes place in the southern hemisphere. Figure 5 shows the trends of the gridded Δf_oF_2 with increasing $\langle ap \rangle_{24\ \mathrm{h}}$ at the southern hemisphere stations. The decreasing trend prevails at higher latitudes (Scott Base, Casey, Terre Adelie, Macquarie Is, and Hobart). With latitude decreasing, the increasing trend gradually appears in winter (see Canberra and Brisbane), while the decreasing trend continues through Darwin in summer. The decreasing trend also becomes unconspicuous at Brisbane, Townsville, and Darwin in equinoxes. As a result, a seasonal difference of the trend is evident at mid-latitudes. With further latitude decreases, however, this seasonal difference disappears. Figure 6 presents the trends of the gridded Δf_oF_2 with increasing $\langle ap \rangle_{24\ \mathrm{h}}$ in the equatorial region. The increasing trend becomes prevailing in all seasons at Manila, Kodaikanal, and Singapore, which is opposite to the cases at higher latitudes.

Figure 7 presents the correlation coefficient between Δf_oF_2 and $\langle ap \rangle_{24\ \mathrm{h}}$ to estimate the statistical significance of the trend. The correlation coefficient has a consistent latitudinal transition with that of the trend. It changes from negative values at higher latitudes into positive values in the equatorial region. The transition also depends on seasons. In general, the absolute value of the correlation coefficient is largest at higher latitudes, secondary in the equatorial region. The correlation is higher in local winter and summer while smaller in equinoxes at mid-latitudes.

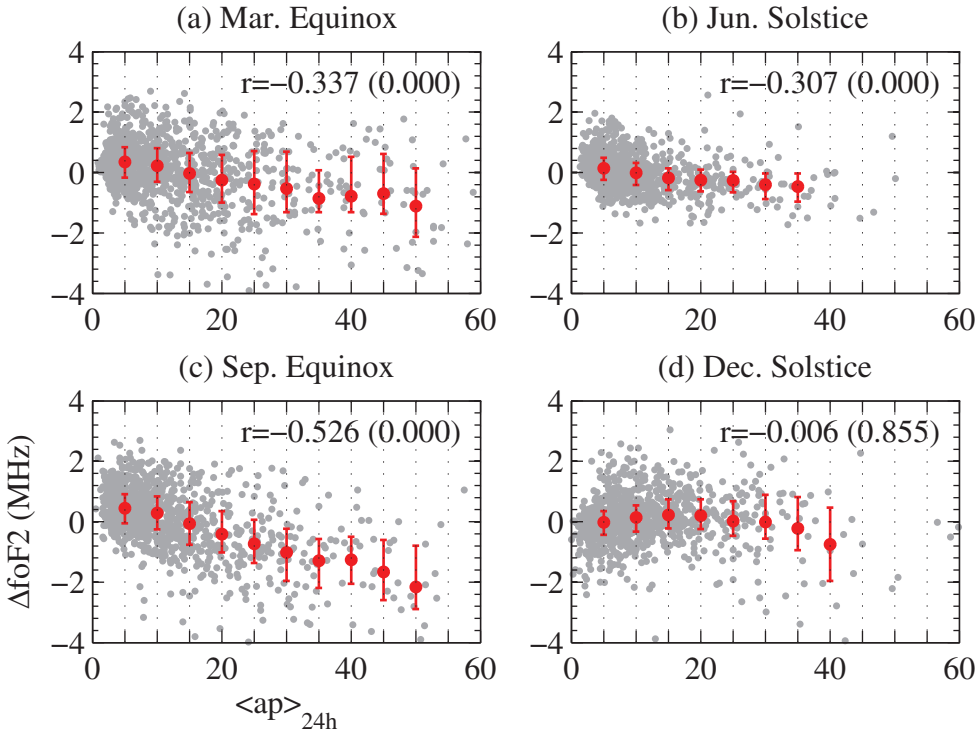

Fig. 3. Scatter plots of the observed minus fitted f_oF_2, Δf_oF_2, versus $<ap>_{24\ h}$ at Petropavlovsk in (a–d) four seasons; the red dots and error bars are mean values and corresponding lower and upper quartiles of gridded Δf_oF_2, respectively. The parameter r is the correlation coefficient between Δf_oF_2 and $<ap>_{24\ h}$, and the number in the parentheses is the corresponding P-value indicating statistical significance of the correlation coefficient.

Higher correlation means a more significant responding trend of f_oF_2 to increasing geomagnetic activity. That is to say; the trend is generally more significant at higher latitudes and in the equatorial region. It is notable that some correlation coefficients are very small or insignificant (marked by the triangles in Fig. 7) at mid-latitudes, especially in equinox seasons. A possible reason is that both the increasing and decreasing trends appear with increasing geomagnetic disturbance levels (for example, the case shown in Fig. 3d, increasing trend turns to decrease trend). The low correlation under this condition does not mean there is no trend. Sometimes the low correlation indeed means no significant trend, for example, the cases at Darwin in equinoxes (Fig. 5).

3 Discussion

The responding trend of f_oF_2 to increasing geomagnetic activity was investigated in detail for weaker geomagnetic disturbances. The trend is statistically significant in the vast majority of cases, while the correlation coefficient between Δf_oF_2 and $<ap>_{24\ h}$ is not very high. Multiple factors are responsible for the lower correlation coefficient. One is that Δf_oF_2 also includes the effects of waves from the lower atmosphere on the ionosphere. Another is that the solar forcing cannot be fully excluded though we tried to remove it as adequately as possible using the improved solar proxy. Moreover, ionospheric responses are likely somewhat chaotic during different weaker geomagnetic disturbances though statistically, there are tendencies. With latitude decreases, the responding trend transits gradually from the decreasing trend dominant at geomagnetic high-latitudes into the increasing trend prevailing in the equatorial region, and the transition depends on seasons. As a result, the trend is seasonally dependent at geomagnetic mid-latitudes.

Many disturbance mechanisms have been proposed to explain the ionospheric storms caused by strong geomagnetic activities, mainly including enhanced particle precipitation and plasma convection at high-latitudes, prompt penetration electric fields, and disturbance dynamo electric fields at low-latitudes, neutral wind disturbances, as well as thermospheric composition changes. Ionospheric responses at different storm stages and in different regions may be dominated by different mechanisms (Prölss, 1995; Buonsanto, 1999; Mendillo, 2006; and references therein). These disturbance mechanisms also can work to some extent for weaker geomagnetic activities. Whereas the relative importance of these mechanisms may be very different for different geomagnetic disturbances, and the effects of different disturbances can interwork owing to the frequent occurrence of weaker geomagnetic activities. Thus, we just focus on the dominant factor responsible for the latitudinally and seasonally dependent responding trends.

The decreasing trends at high latitudes are contrary to the effect of enhanced polar particle precipitation that causes increasing ionization. Enhanced polar plasma convection can redistribute the ionospheric plasma to form complex and variable spatial structures of plasma density at high latitudes

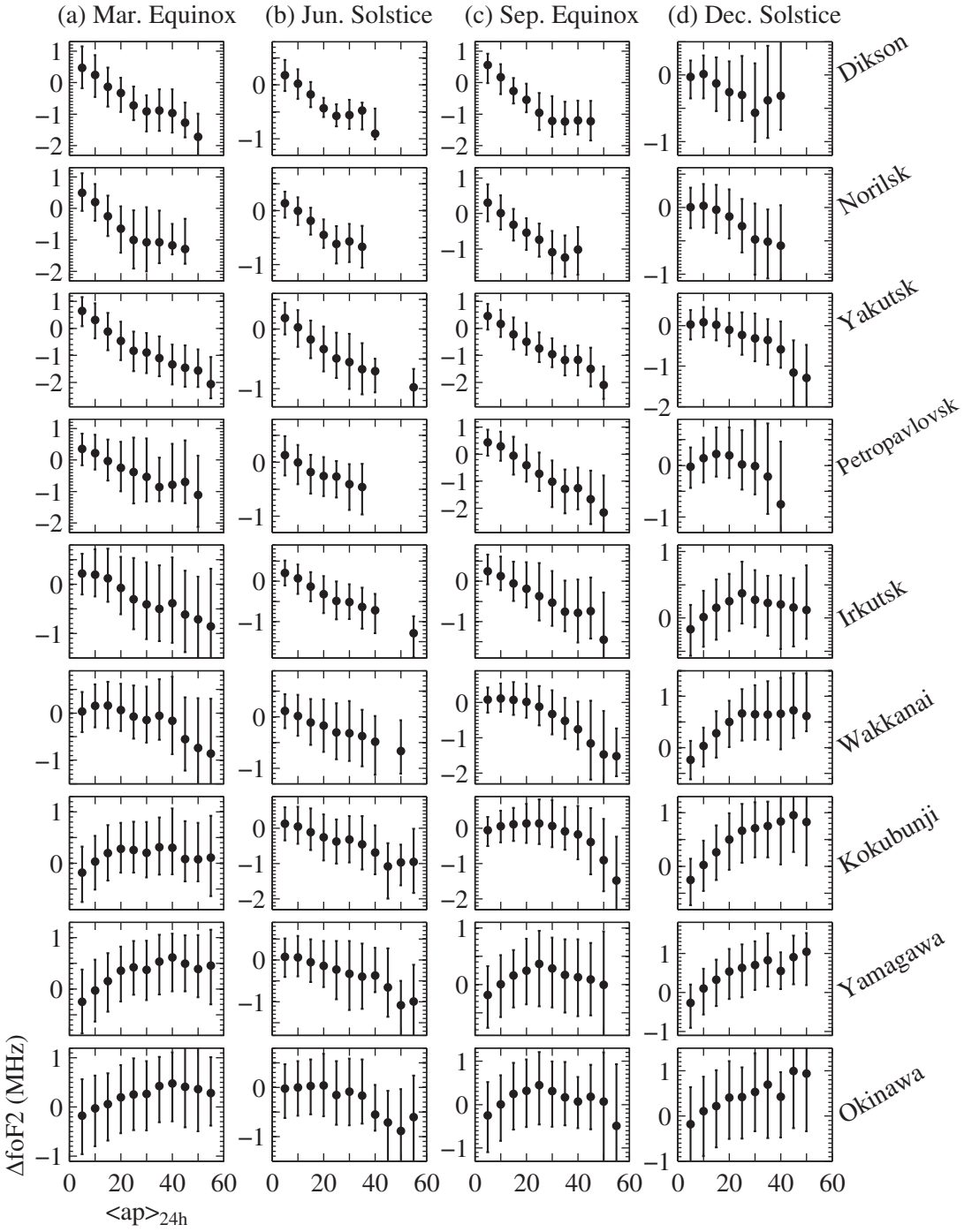

Fig. 4. Variations of the gridded mean Δf_oF_2 with increasing $<ap>_{24\ h}$ at the northern hemisphere stations (from top to bottom: Dikson, Norilsk, Yakutsk, Petropavlovsk, Irkutsk, Wakkanai, Kokubunji, Yamagawa, and Okinawa); the error bars indicate the lower and upper quartiles of the gridded Δf_oF_2. (a–d) present the variations under the seasonal conditions of March equinox, June Solstice, September equinox, and December solstice, respectively.

(Prölss, 1995). It is more important for the global ionosphere that the polar convection can significantly disturb the neutral atmosphere by Joule heating to further affect the ionosphere by photochemical and dynamic processes. With geomagnetic activity increases, the increasing Joule heating enhances high-latitude atmospheric upwelling to reduce thermospheric $[O]/[N_2]$ (e.g., Rishbeth et al., 1987; Fuller-Rowell et al., 1994; Field & Rishbeth, 1997), which results in declining F_2-layer electron density at high-latitudes. The prevailing decreasing trend of f_oF_2 to increasing geomagnetic activity at high latitudes is consistent with this thermospheric composition disturbance mechanism.

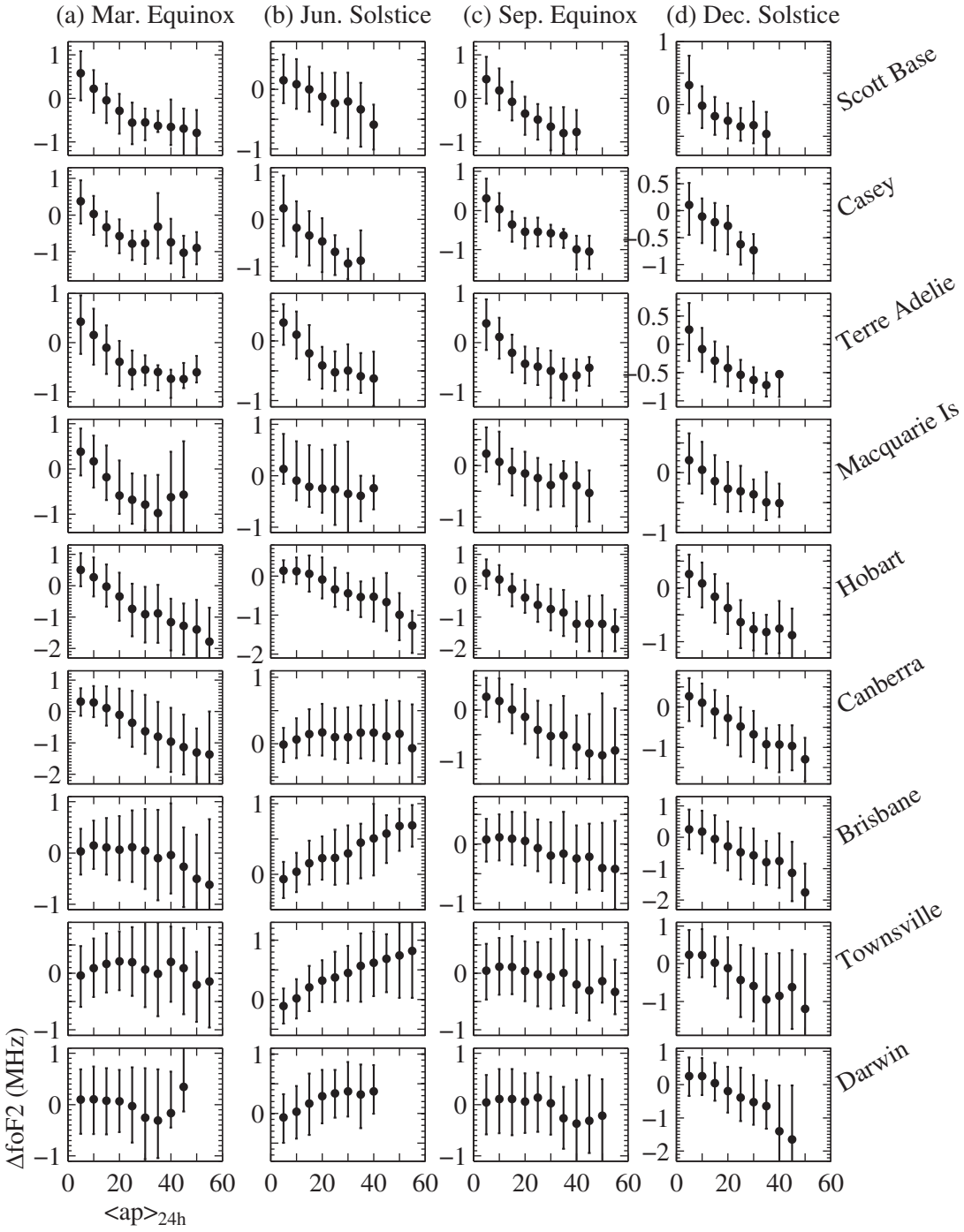

Fig. 5. Same as Figure 4 but for the southern hemisphere stations (from top to bottom: Scott Base, Casey, Terre Adelie, Macquarie Is, Hobart, Canberra, Brisbane, Townsville, and Darwin).

The polar upwelling of the hot and molecule-enriched air induces an atmospheric high-pressure zone, where thermospheric composition bulge forms. This high-pressure zone would expand equatorwards to further affect the mid-and low-latitude ionosphere by changing thermospheric composition and neutral winds, i.e., the storm-induced circulation (e.g., Rishbeth, 1975). For weaker geomagnetic activities, nevertheless, this equatorward expansion should not be very intense. Meanwhile, the composition bulge zone interacts with the background thermospheric circulation. The polar composition disturbance is superimposed on the background circulation to transport the molecule-enriched air (e.g., Fuller-Rowell et al., 1994, 1996; Field et al., 1998; Buonsanto, 1999). The background circulation will reach a new equilibrium to form an altered circulation (Fuller-Rowell et al., 1994) if the storm energy input remains continuously. That is expected to be

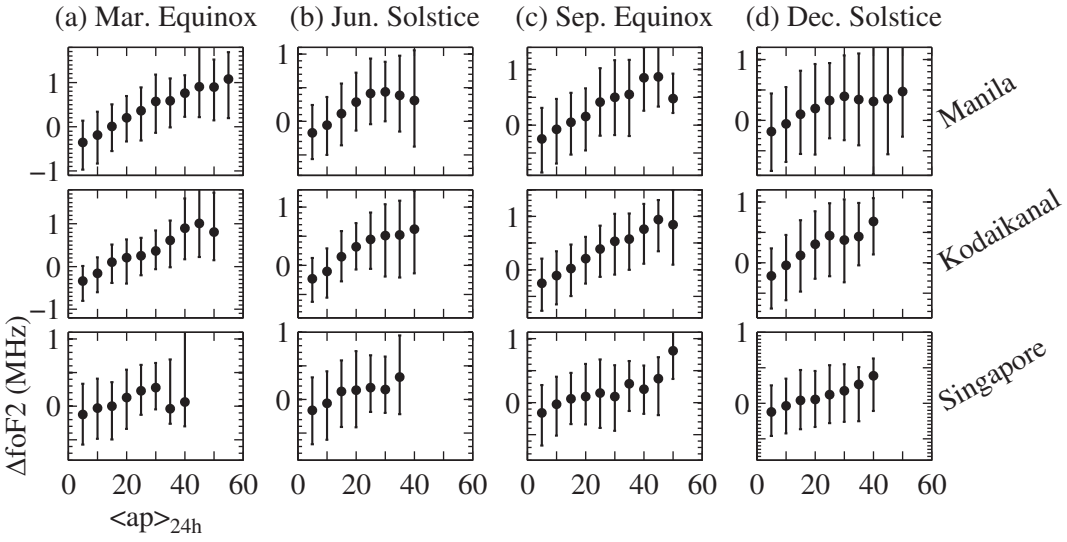

Fig. 6. Same as Figure 4 but for the equatorial stations (from top to bottom: Manila, Kodaikanal, and Singapore).

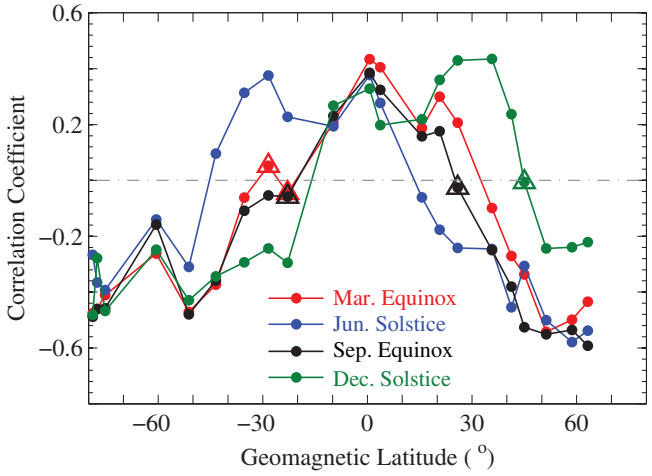

Fig. 7. Latitude variations of the correlation coefficient between Δf_oF_2 and $<ap>_{24\ h}$; the red, blue, black, and green lines correspond to the seasonal conditions of March equinox, June Solstice, September equinox, and December solstice, respectively. The dots surrounded by triangles indicate low statistical significance ($P > 0.01$) of the correlation coefficient.

idoneous to some extent for the frequent weaker geomagnetic activities. In equinox seasons, the equatorward circulation can be reinforced at nightside by the frequent weaker geomagnetic activities to transport the molecule-enriched air so that the mid-latitude [O]/[N_2] decreases. Atmospheric downwelling gradually arises far away from the polar region owing to the encounter of two altered circulation cells, which increases the [O]/[N_2] instead at low-latitudes through increasing the O density relative to N_2 and O_2 (e.g., Rishbeth et al., 1987; Fuller-Rowell et al., 1994; Buonsanto, 1999). In solstice seasons, the prevailing summer to winter circulation transports the molecule-enriched air equatorwards in the summer hemisphere while restricting the composition bulge zone expansion in the winter hemisphere (e.g., Fuller-Rowell et al., 1996; Buonsanto, 1999). The downwelling also occurs far away from the summer polar region to increase the [O]/[N_2] at low-latitudes and winter mid-latitudes. The molecule-enriched air can be transported farther in solstice seasons than in equinox seasons when two circulation cells collide at low latitudes. The altered thermospheric composition can corotate to dayside and affect the mid-and low-latitude ionosphere, though the background circulation reverses in the daytime. The decreasing [O]/[N_2] depresses the daytime F_2-layer electron density, and the increasing [O]/[N_2] enhances it.

The morphology of the latitudinal transition of the responding trend can be explained by the composition disturbance induced by the polar upwelling and the altered background circulation. In equinox seasons, the polar composition disturbance is transported equatorwards by the circulation, which causes the extension of the polar decreasing trend to mid-latitudes. The decreasing trend gradually changes into an increasing trend with the presence of the downwelling at low latitudes. In solstice seasons, the polar composition disturbance is transported to lower latitudes by the summer to winter circulation to cause the equatorward extension of the decreasing trend in the summer hemisphere, while the polar upwelling induced composition bulge and the corresponding decreasing trend are restricted at higher latitudes by the summer to winter circulation in the winter hemisphere. The downwelling of the summer to winter circulation increases the [O]/[N_2] to cause the increasing trend at low-latitudes and winter mid-latitudes. It should be noted that the seasonal dependence of the mid-latitude trend is similar to that of ionospheric storm effects, i.e., negative storms often take place in summer while positive storms prevail in winter. The thermospheric composition disturbance was suggested to be the mechanism responsible for the seasonally dependent storm effects (e.g., Fuller-Rowell et al., 1996; Field et al., 1998).

Other disturbance mechanisms cannot in extenso explain the morphology of the trend. The polar high-pressure zone can reduce the intensity of daytime poleward wind when geomagnetic activity enhances. This neutral wind disturbance should cause increasing f_oF_2 at mid-latitudes in all seasons, inconsistent

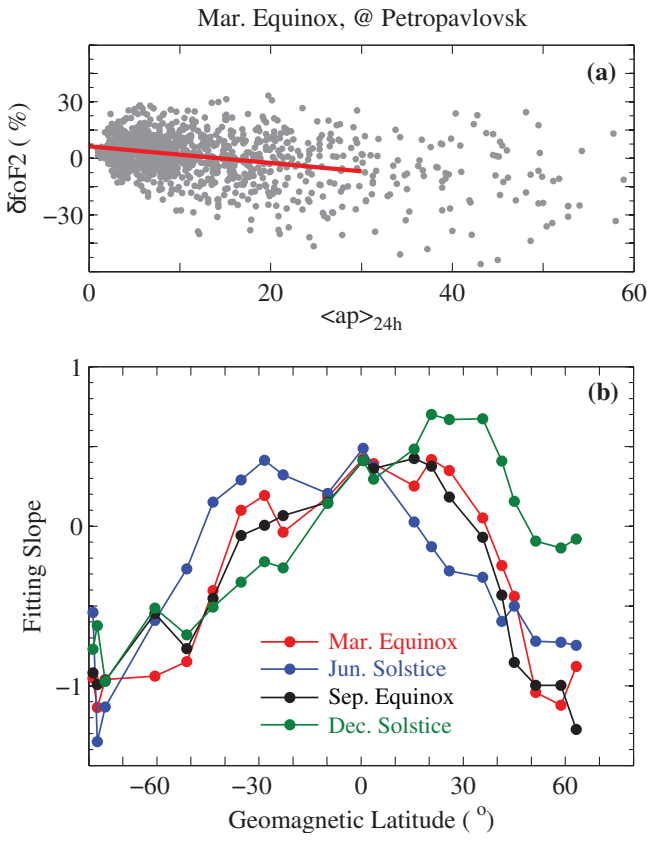

Fig. 8. (a) Scatter plots of the percentage deviation of observed f_oF_2 from the fitted values, δf_oF_2, versus $\langle ap\rangle_{24\ h}$ at Petropavlovsk in March equinox season; the red line is the linear fitting of the dots for the geomagnetic activity level of $\langle ap\rangle_{24\ h}<30$. (b) Latitude variations of the fitting slope of δf_oF_2 versus $\langle ap\rangle_{24\ h}$; the red, blue, black, and green lines correspond to the seasonal conditions of March equinox, June Solstice, September equinox, and December solstice, respectively.

with the seasonally dependent trends at mid-latitudes. Nevertheless, neutral wind disturbance may modulate the mid-latitude trends more or less. It may reinforce the increasing trend in winter while reducing the decreasing trend in other seasons at mid-latitudes. Electric field disturbance is usually important for the low-latitude ionosphere (e.g., Tsurutani et al., 2006b, 2008). Inconsistent with the prevalence of increasing trend at low-latitudes, however, it should result in opposite f_oF_2 perturbations between the EIA trough and crests. Thus, the low-latitude increasing trend should be attributed to the composition disturbance of increasing [O]/[N_2], which was suggested to be capable of resulting in positive ionospheric storms at low-latitudes during strong geomagnetic disturbances (e.g., Fuller-Rowell et al., 1994; Prölss, 1995; Field et al., 1998; Buonsanto, 1999).

It can be inferred from the above analysis that the responding intensity of f_oF_2 to weaker geomagnetic activities is likely related to the composition disturbance degree. We estimated the responding intensity in terms of the fitting slope of the percentage deviation of observed from fitted f_oF_2 versus $\langle ap\rangle_{24\ h}$. The fitting slope of $\langle ap\rangle_{24\ h}<30$ segment was used in view of that the data are mainly at the lower geomagnetic activity level of $\langle ap\rangle_{24\ h}<30$, and the trend sometimes reverses if geomagnetic activity further increases. Figure 8a illustrates the slope fitted from the percentage deviation of f_oF_2 versus $\langle ap\rangle_{24\ h}$ as an example. Figure 8b shows the slopes at all stations and in all seasons to present the latitudinal dependence of the responding intensity. In general, the absolute value of the slope is largest at higher latitudes, which is consistent with that the responses of f_oF_2 to weaker geomagnetic activities should be strongest near the source region of the composition disturbance. The composition disturbance of decreasing [O]/[N_2] should be gradually declining away from the high-latitude disturbance source region, while the contrary composition disturbance may enhance the [O]/[N_2] rather than decrease it at low-latitudes owing to the presence of downwelling. Correspondingly, the absolute value of the slope declines first and then trends to increase with decreasing latitude. Thus, the result of Figure 8b further supports the composition disturbance mechanism.

4 Summary

The responses of the low- to high-latitude ionosphere to the frequent weaker geomagnetic activities were statistically investigated. The responding trend of f_oF_2 to increasing geomagnetic activity was obtained for different ionosonde stations and for different seasons to present the morphology of the trend. The responding trend is statistically significant in the vast majority of cases, and it remarkably depends on latitudes. The decreasing trend is dominant at higher latitudes, and the increasing trend prevails in the equatorial region. With latitude decreases, the trend gradually transits from the high-latitude decreasing trend to the equatorial increasing trend. This latitudinal transition is seasonally dependent. It occurs first in winter and then in equinoxes with decreasing latitude, while the decreasing trend can keep through near the equatorial region in summer. As a result, the trend shows remarkable seasonal differences at mid-latitudes, i.e., the decreasing trend in summer and the increasing trend in winter (sometimes the trend is not distinct in equinoxes). In general, the trend is more significant at higher latitudes and in the equatorial region than at mid-latitudes, and the responding intensity of f_oF_2 to increasing geomagnetic activity is largest at higher latitudes. Geomagnetic disturbances can modulate the ionosphere through multiple mechanisms. For the frequent weaker geomagnetic activities, nevertheless, the results suggest that the thermospheric composition disturbance caused by both the polar thermospheric upwelling and the altered background circulation is primarily responsible for the morphology of the responding trend.

Acknowledgements. The authors acknowledge the Space Physics Interactive Data Resource (SPIDR) for providing the ionosonde measurements; the f_oF_2 data can be accessed at the WDC for Geophysics, Beijing (https://doi.org/10.12197/2021GA018). The ionosonde measurements at Okinawa, Yamagawa, Kokubunji, and Wakkanai are available at https://wdc.nict.go.jp/IONO/HP2009/ISDJ/manual_txt-E.html; the SOHO/SEM daily EUV flux can be downloaded from https://dornsifecms.usc.edu/space-sciences-center/download-sem-data; the $F_{10.7}$ index can be obtained at https://www.ngdc.noaa.gov/stp/space-weather/solar-data/solar-features/solar-radio/noontime-flux/penticton/penticton_adjusted; the

ap index is available at https://www.ngdc.noaa.gov/geomag/indices/kp_ap.html. This research was supported by the National Natural Science Foundation of China (41922029, 42030202, and 41904140) and Youth Innovation Promotion Association, CAS (grant No. Y202021). The editor thanks Jan Lastovicka and an anonymous reviewer for their assistance in evaluating this paper.

References

Anderson CN. 1928. Correlation of long wave transatlantic radio transmission with other factors affected by solar activity. *Proc IRE* **16**: 297–347. https://doi.org/10.1109/JRPROC.1928.221400.

Buonsanto MJ. 1999. Ionospheric storm – A review. *Space Sci Rev* **88**: 563–601. https://doi.org/10.1023/A:1005107532631.

Buresova D, Lastovicka J, Hejda P, Bochnicek J. 2014. Ionospheric disturbances under low solar activity conditions. *Adv Space Res* **54**: 185–196. https://doi.org/10.1016/j.asr.2014.04.007.

Chen Y, Liu L, Le H. 2008. Solar activity variations of nighttime ionospheric peak electron density. *J Geophys Res* **113**: A11306. https://doi.org/10.1029/2008JA013114.

Chen Y, Liu L, Wan W. 2011. Does the $F_{10.7}$ index correctly describe solar EUV flux during the deep solar minimum of 2007–2009? *J Geophys Res* **116**: A04304. https://doi.org/10.1029/2010JA016301.

Chen Y, Liu L, Wan W. 2012. The discrepancy in solar EUV-proxy correlations on solar cycle and solar rotation timescales and its manifestation in the ionosphere. *J Geophys Res* **117**: A03313. https://doi.org/10.1029/2011JA017224.

Chen Y, Liu L, Le H, Wan W. 2014a. Geomagnetic activity effect on the global ionosphere during the 2007–2009 deep solar minimum. *J Geophys Res (Space Phys)* **119**: 3747–3754. https://doi.org/10.1002/2013JA019692.

Chen Y, Liu L, Le H, Wan W. 2014b. How does ionospheric TEC vary if solar EUV irradiance continuously decreases? *Earth Planet Space* **66**: 52. https://doi.org/10.1186/1880-5981-66-52.

Chen Y, Liu L, Le H, Zhang H. 2015. Discrepant responses of the global electron content to the solar cycle and solar rotation variations of EUV irradiance. *Earth Planet Space* **67**: 80. https://doi.org/10.1186/s40623-015-0251-x.

Chen Y, Liu L, Le H, Wan W. 2018. Responses of solar irradiance and the ionosphere to an intense activity region. *J Geophys Res (Space Phys)* **123**: 2116–2126. https://doi.org/10.1002/2017JA024765.

Coley WR, Heelis RA. 2012. Response of the equatorial topside ionosphere to 27-day variations in solar EUV input during a low solar activity period using C/NOFS. *J Geophys Res* **117**: A03330. https://doi.org/10.1029/2011JA017301.

Danilov AD. 2013. Ionospheric F-region response to geomagnetic disturbances. *Adv Space Res* **52**: 343–366. https://doi.org/10.1016/j.asr.2013.04.019.

Elias AG. 2014. Filtering ionosphere parameters to detect trends linked to anthropogenic effects. *Earth Planet Space* **66**: 113. https://doi.org/10.1186/1880-5981-66-113.

Emmert JT, Mannucci AJ, McDonald SE, Vergados P. 2017. Attribution of interminimum changes in global and hemispheric total electron content. *J Geophys Res (Space Phys)* **122**: 2424–2439. https://doi.org/10.1002/2016JA023680.

Fares Saba MM, Gonzalez WD, Clúa de Gonzalez AL. 1997. Relationships between the AE, ap and Dst indices near solar minimum (1974) and at solar maximum (1979). *Ann Geophys* **15**: 1265–1270. https://doi.org/10.1007/s00585-997-1265-x.

Field PR, Rishbeth H. 1997. The response of the ionospheric F2-layer to geomagnetic activity: an analysis of worldwide data. *J Atmos Sol Terr Phys* **59**: 163–180. https://doi.org/10.1016/S1364-6826(96)00085-5.

Field PR, Rishbeth H, Moffett RJ, Idenden DW, Fuller-Rowell TJ, Millward GH, Aylward AD. 1998. Modelling composition changes in F-layer storms. *J Atmos Sol Terr Phys* **60**: 523–543. https://doi.org/10.1016/S1364-6826(97)00074-6.

Forbes JM, Palo SE, Zhang X. 2000. Variability of the ionosphere. *J Atmos Sol Terr Phys* **62**: 685–693. https://doi.org/10.1016/S1364-6826(00)00029-8.

Fuller-Rowell TJ, Codrescu MV, Moffett RJ, Quegan S. 1994. Response of the thermosphere and ionosphere to geomagnetic storms. *J Geophys Res* **99**: 3893–3914. https://doi.org/10.1029/93JA02015.

Fuller-Rowell TJ, Codrescu MV, Rishbeth H, Moffett RJ, Quegan S. 1996. On the seasonal response of the thermosphere and ionosphere to geomagnetic storms. *J Geophys Res* **101**: 2343–2353. https://doi.org/10.1029/95JA01614.

Gonzalez WD, Joselyn JA, Kamide Y, Kroehl HW, Rostoker G, Tsurutani BT, Vasyliunas VM. 1994. What is a geomagnetic storm? *J Geophys Res* **99**: 5771–5792. https://doi.org/10.1029/93JA02867.

Gonzalez WD, Tsurutani BT, Clúa de Gonzalez AL. 1999. Interplanetary origin of geomagnetic storms. *Space Sci Rev* **88**: 529–562. https://doi.org/10.1023/A:1005160129098.

Hafstad LR, Tuve MA. 1929. Note on Kennelly-Heaviside layer observations during a magnetic storm. *Terr Magn Atmos Electr* **34**: 39–44. https://doi.org/10.1029/TE034i001p00039.

Judge DL, McMullin DR, Ogawa HS, Hovestadt D, Klecker B, et al. 1998. First solar EUV irradiances obtained from SOHO by the CELIAS/SEM. *Sol Phys* **177**: 161–173. https://doi.org/10.1023/A:1004929011427.

Lei J, Thayer JP, Forbes JM, Wu Q, She C, Wan W, Wang W. 2008. Ionosphere response to solar wind high-speed streams. *Geophys Res Lett* **35**: L19105. https://doi.org/10.1029/2008GL035208.

Liu L, Wan W, Ning B, Pirog OM, Kurkin VI. 2006. Solar activity variations of the ionospheric peak electron density. *J Geophys Res* **111**: A08304. https://doi.org/10.1029/2006JA011598.

Liu L, Zhao B, Wan W, Ning B, Zhang M-L, He M. 2009. Seasonal variations of the ionospheric electron densities retrieved from constellation observing system for meteorology, ionosphere, and climate mission radio occultation measurements. *J Geophys Res* **114**: A02302. https://doi.org/10.1029/2008JA013819.

Mayaud PN. 1980. Derivation, meaning, and use of geomagnetic indices. *Geophys Monogr* **22**, AGU, Washington DC. https://doi.org/10.1029/GM022.

Mendillo M. 2006. Storms in the ionosphere: Patterns and processes for total electron content. *Rev Geophys* **44**: RG4001. https://doi.org/10.1029/2005RG000193.

Mendillo M, Rishbeth H, Roble RG, Wroten J. 2002. Modelling F2-layer seasonal trends and day-to-day variability driven by coupling with the lower atmosphere. *J Atmos Sol Terr Phys* **64**: 1911–1931. https://doi.org/10.1016/S1364-6826(02)00193-1.

Min K, Park J, Kim H, Kim V, Kil H, Lee J, Rentz S, Lühr H, Paxton L. 2009. The 27-day modulation of the low-latitude ionosphere during a solar maximum. *J Geophys Res* **114**: A04317. https://doi.org/10.1029/2008JA013881.

Pedatella NM, Lei J, Thayer JP, Forbes JM. 2010. Ionosphere response to recurrent geomagnetic activity: Local time dependency. *J Geophys Res* **115**: A02301. https://doi.org/10.1029/2009JA014712.

Prölss GW. 1995. Ionospheric F-region storms. In: *Handbook of atmospheric electrodynamics*, Vol. **II**, CRC Press, Boca Raton, FL, pp. 195–248. https://doi.org/10.1201/9780203713297.

Rich FJ, Sultan PJ, Burke WJ. 2003. The 27-day variations of plasma densities and temperatures in the topside ionosphere. *J Geophys Res* **108(A7)**: 1297. https://doi.org/10.1029/2002JA009731.

Richards PG, Fennelly JA, Torr DG. 1994. EUVAC: A solar EUV flux model for aeronomic calculations. *J Geophys Res* **99**: 8981–8992. https://doi.org/10.1029/94JA00518.

Rishbeth H. 1975. F-region storms and thermospheric circulation. *J Atmos Terr Phys* **37**: 1055–1064. https://doi.org/10.1016/0021-9169(75)90013-6.

Rishbeth H, Fuller-Rowell TJ, Rees D. 1987. Diffusive equilibrium and vertical motion in the thermosphere during a severe magnetic storm: A computational study. *Planet Space Sci* **35(9)**: 1157–1165. https://doi.org/10.1016/0032-0633(87)90022-5.

Rishbeth H, Mendillo M. 2001. Patterns of F2-layer variability. *J Atmos Sol Terr Phys* **63**: 1661–1680. https://doi.org/10.1016/S1364-6826(01)00036-0.

Sethi NK, Goel MK, Mahajan KK. 2002. Solar cycle variations of foF2 from IGY to 1990. *Ann Geophys* **20**: 1677–1685. https://doi.org/10.5194/angeo-20-1677-2002.

Solomon SC, Qian L, Burns AG. 2013. The anomalous ionosphere between solar cycles 23 and 24. *J Geophys Res (Space Phys)* **118**: 6524–6535. https://doi.org/10.1002/jgra.50561.

Solomon SC, Qian L, Mannucci AJ. 2018. Ionospheric electron content during solar cycle 23. *J Geophys Res (Space Phys)* **123**: 5223–5231. https://doi.org/10.1029/2018JA025464.

Tsurutani BT, Gonzalez WD, Gonzalez ALC, Guarnieri FL, Gopalswamy N, et al. 2006a. Corotating solar wind streams and recurrent geomagnetic activity: A review. *J Geophys Res* **111**: A07S01. https://doi.org/10.1029/2005JA011273.

Tsurutani BT, Mannucci AJ, Iijima BA, Komjathy A, Saito A, et al. 2006b. Dayside ionospheric (GPS) response to corotating solar wind streams. In: *Recurrent magnetic storms: Corotating solar wind streams*, Tsurutani B, McPherron R, Gonzalez W, Lu G, Sobral JHA, Gopalswamy N (Eds.), American Geophysical Union, Washington, DC, pp. 245–270. https://doi.org/10.1029/167GM20.

Tsurutani BT, McPherron RL, Gonzalez WD, Lu G, Sobral JHA, Gopalswamy N. 2006c. Introduction to special section on corotating solar wind streams and recurrent geomagnetic activity. *J Geophys Res* **111**: A07S00. https://doi.org/10.1029/2006JA011745.

Tsurutani BT, Verkhoglyadova OP, Mannucci AJ, Saito A, Araki T, et al. 2008. Prompt penetration electric fields (PPEFs) and their ionospheric effects during the great magnetic storm of 30–31 October 2003. *J Geophys Res* **113**: A05311. https://doi.org/10.1029/2007JA012879.

Tulasi Ram S, Lei J, Su S-Y, Liu CH, Lin CH, Chen WS. 2010. Dayside ionospheric response to recurrent geomagnetic activity during the extreme solar minimum of 2008. *Geophys Res Lett* **37**: L02101. https://doi.org/10.1029/2009GL041038.

Vaishnav R, Jacobi C, Berdermann J. 2019. Long-term trends in the ionospheric response to solar extreme-ultraviolat variations. *Ann Geophys* **37**: 1141–1159. https://doi.org/10.5194/angeo-37-1141-2019.

Wang W, Lei J, Burns AG, Qian L, Solomon SC, Wiltberger M, Xu J. 2011. Ionospheric day-to-day variability around the whole heliosphere interval in 2008. *Sol Phys* **274**: 457–472. https://doi.org/10.1007/s11207-011-9747-0.

Woods TN, Eparvier FG, Bailey SM, Chamberlin PC, Lean J, Rottman GJ, Solomon SC, Tobiska WK, Woodraska DL. 2005. Solar EUV experiment (SEE): Mission overview and first results. *J Geophys Res* **110**: A01312. https://doi.org/10.1029/2004JA010765.

Xu J, Ma R, Wang W. 2012. Terannual variation in the F2 layer peak electron density (NmF2) at middle latitudes. *J Geophys Res* **117**: A01308. https://doi.org/10.1029/2011JA017191.

Cite this article as: Chen Y, Liu L, Le H, Zhang H & Zhang R 2022. Responding trends of ionospheric F_2-layer to weaker geomagnetic activities. *J. Space Weather Space Clim.* **12**, 6. https://doi.org/10.1051/swsc/2022005.